

Parametric resonance energy exchange and induction phenomenon in a one-dimensional nonlinear oscillator chain

K. Yoshimura*

NTT Communication Science Laboratories, 2-4, Hikaridai, Seika-cho, Soraku-gun, Kyoto 619-0237, Japan

(Received 10 May 2000)

We study analytically the induction phenomenon in the Fermi-Pasta-Ulam β oscillator chain under initial conditions consisting of single mode excitation. Our study is based on the analytical computation of the largest characteristic exponent of an approximate version of the variational equation. The main results can be summarized as follows: (1) the energy density ϵ scaling of the induction time T is given by $T \sim \epsilon^{-1}$, and T becomes smaller for higher-frequency mode excitation; (2) there is a threshold energy density ϵ_c such that the induction time diverges when $\epsilon < \epsilon_c = \pi^2/6\beta N^2$, where N is the system size and β the nonlinearity parameter, and this expression for ϵ_c is correct in the limit $N \rightarrow \infty$; (3) the threshold ϵ_c vanishes as $\epsilon_c \sim N^{-2}$ in the limit $N \rightarrow \infty$; (4) the threshold ϵ_c does not depend on the mode number k that is excited in the initial condition; (5) the two modes $k \pm m$ have the largest exponential growth rate, and m increases with increasing ϵ as $m/N = \sqrt{3}\beta\epsilon/\pi$. The above analytical results are thoroughly verified in numerical experiments. Moreover, we discuss the energy exchange process after the induction period in some energy density regimes, based on the numerical results.

PACS number(s): 05.45.-a, 45.20.Jj, 05.20.-y

I. INTRODUCTION

Fermi, Pasta, and Ulam (FPU) first studied the relaxation to equilibrium of one-dimensional nonlinear oscillator chains [1]. They chose an initial condition far from equilibrium, giving all energy to the lowest-frequency normal mode, and then numerically integrated the equations of motion. It is well known that the expected chaotic energy exchange among the normal modes did not occur within their observation time scale, but quasiperiodic normal mode oscillation including only a few low-frequency modes was observed. Their numerical results showed that the relaxation to equilibrium is not an obvious consequence of the nonexistence of analytic first integrals of the motion other than the energy.

Since the appearance of their ground-breaking work, many studies of the chaotic dynamics of such systems have been carried out in order to understand their relaxation properties. For the FPU α model, which has cubic nonlinearity in its Hamiltonian, Casetti *et al.* have recently reexamined the relaxation properties by carrying out extensive numerical experiments with the aid of modern high-performance computers [2]. An interesting result they found is that at a certain threshold in energy density ϵ ($\epsilon \equiv E/N$ is the energy per degree of freedom), the largest Lyapunov exponent rapidly decreases and the relaxation time seems to diverge. That is, the motion seems to be quite regular below the threshold while it is chaotic (although very weakly) above the threshold. The threshold was also shown to become smaller as the number N of degrees of freedom increases. A theoretical study of the N scaling of the threshold based on an approximate resonant Hamiltonian suggests that the threshold energy density vanishes in the thermodynamic limit $N \rightarrow \infty$ [3]. However, it is still not very clear whether the largest Lyapunov exponent drops exactly to zero and the relaxation time

really diverges at the threshold. It may be necessary to obtain more accurate theoretical results for the threshold.

A model more extensively studied in the literature is the FPU β model, which has quartic nonlinearity in its Hamiltonian. A simple initial condition often used in those studies is that involving only a single-mode excitation or a narrow-packet excitation. In such a condition, only a single normal mode of some wave number k or a wave packet of small size δk with mean wave number k ($\delta k/k \ll 1$) is initially excited. Izrailev and Chirikov applied the resonance overlap criterion under this initial condition and indicated that above a threshold energy density the chaotic energy exchange with the other modes occurs in a short time [4] (see also Refs. [5,6]). They also showed that, in the regime of small k (i.e., $k \ll N$), the threshold decreases as the wave number k increases. This implies that the time scale for the chaotic energy exchange to occur becomes smaller when a mode of larger k is initially excited. Recently, the k dependence of the time scale for chaotic energy exchange has been studied in detail [7,8]. A quite different result was found for a rather large k mode excitation. The time scale exhibited an intricate k dependence in a sufficiently large energy density regime: the chaotic energy exchange is enhanced intermittently in some specific wave number ranges and the time scale then becomes smaller, while for wave numbers within a certain range the mode oscillation is extremely stable and the time scale is very large. It was theoretically shown that parametric resonance instability among four specific modes plays a crucial role in this strong k dependence of the time scale [8]. Pettini and his collaborators proposed a new interpretation of the threshold energy density, which distinguishes weak and strong chaos [9,10]. They showed that below the threshold the relaxation time rapidly increases and the largest Lyapunov exponent rapidly decreases as ϵ decreases. They called the energy density threshold a *strong stochasticity threshold* (SST). A SST has also been shown to exist in some other oscillator chain models besides the FPU β model [11]. A detailed study of the chaoticity transition between

*Electronic address: kazuyuki@cslab.kecl.ntt.co.jp

weak and strong chaos was done by using a Riemannian geometric description of Hamiltonian chaos [12–15]. Recently, De Luca *et al.* have studied the same model and given a very detailed picture of the motion in the low-energy regime [16]. In spite of all the above work, the dynamics of the FPU β model in the relaxation process is not yet fully understood. In particular, a theoretical result that appropriately describes the dynamics in the relaxation process is still lacking.

A well known dynamical phenomenon relevant to the relaxation from single-mode excitation in the small energy density regime is the *induction phenomenon*, which was found for the FPU β model by Ooyama *et al.* [17] (see also [18,19]). In the induction phenomenon, energy initially supplied to a single mode remains in the initially excited mode during a certain period called the *induction period*, and then abruptly transfers to some of the other modes. A theoretical study of this phenomenon has also been presented based on a Mathieu equation stability analysis [19]. Recently, Christie and Henry pointed out that this analysis is unsatisfactory, so they carried out an analysis based on a frequency shifted perturbation [20]. Their analysis fully explains the mode energy pattern in the very early stage of the induction period. However, it fails to explain the exponential growth of the mode energies. In this paper, we present a theoretical study based on a stability analysis of *coupled* Hill equations. Our analysis explains the exponential growth of the mode energies, correctly identifies the fastest growing modes, scales the induction time with the energy density, and shows that the induction period diverges at a threshold energy density, which is independent of the initially excited mode's wave number k and vanishes as N^{-2} in the limit $N \rightarrow \infty$. Our theoretical results appropriately describe the mode dynamics during the induction period.

The present paper is organized as follows. In Sec. II, we describe the FPU β model and introduce normal mode coordinates. In Sec. III, we describe the relationship between the mode energy exchange in the induction phenomenon and the exponential instability of nearby orbits. An approximate version of a variational equation, which we call an average variational equation, is proposed for examining the exponential instability. In Sec. IV, we analytically compute the exponential instability rate using the averaging method and derive some analytical results on the induction phenomenon. In Sec. V, we verify these results in numerical experiments. Conclusions are offered in Sec. VI.

II. FPU β MODEL AND NORMAL MODE

In this section, we describe the FPU β model and the normal modes. Our investigation is of the dynamical model

described by the Hamiltonian

$$H = \frac{1}{2} \sum_{i=1}^{N-1} p_i^2 + \sum_{i=1}^N \left[\frac{1}{2} (q_i - q_{i-1})^2 + \frac{\beta}{4} (q_i - q_{i-1})^4 \right]. \quad (1)$$

This is referred to as the FPU β model. This Hamiltonian describes a one-dimensional nonlinear oscillator chain with nearest neighbor interaction. We employ fixed-end boundary conditions, i.e., $q_0 = q_N = 0$. The parameter β represents the nonlinear coupling strength. We will set $\beta = 1$ in later numerical experiments. We define the energy density ϵ as $\epsilon = E/N$, where E is the total energy of the system. The equations of motion derived from the Hamiltonian (1) are

$$\frac{d^2 q_i}{dt^2} = q_{i+1} + q_{i-1} - 2q_i + \beta [(q_{i+1} - q_i)^3 - (q_i - q_{i-1})^3]. \quad (2)$$

The transformation $\mathbf{q} \rightarrow \mathbf{Q}$ defined by

$$q_i = \sqrt{\frac{2}{N}} \sum_{k=1}^{N-1} Q_k \sin\left(\frac{\pi k}{N} i\right), \quad (i=1, 2, \dots, N-1) \quad (3)$$

gives the normal modes of the corresponding linear system. Here, Q_k is the amplitude of the k th normal mode. The characteristic frequency of the k th normal mode is given by

$$\omega_k = 2 \sin\left(\frac{\pi k}{2N}\right). \quad (4)$$

In terms of the normal mode coordinates \mathbf{Q} and their conjugate momenta \mathbf{P} ($=\dot{\mathbf{Q}}$), the Hamiltonian (1) is rewritten as

$$H = \sum_{k=1}^{N-1} \left(\frac{1}{2} P_k^2 + \frac{1}{2} \omega_k^2 Q_k^2 \right) + \frac{\beta}{8N} \sum_{k_1, k_2, k_3, k_4=1}^{N-1} \omega_{k_1} \omega_{k_2} \omega_{k_3} \omega_{k_4} \times Q_{k_1} Q_{k_2} Q_{k_3} Q_{k_4} D(k_1, k_2, k_3, k_4), \quad (5)$$

where $D(k_1, k_2, k_3, k_4)$ represents the selection rule defining the interaction among the normal modes. It is explicitly written as

$$\begin{aligned} D(k_1, k_2, k_3, k_4) = & \delta(k_1 + k_2, k_3 + k_4) + \delta(k_1 + k_3, k_2 + k_4) + \delta(k_1 + k_4, k_2 + k_3) + \delta(k_1 + k_2 + k_3, k_4) + \delta(k_1 + k_2 + k_4, k_3) \\ & + \delta(k_1 + k_3 + k_4, k_2) + \delta(k_2 + k_3 + k_4, k_1) - \delta(k_1 + k_2 + k_3 + k_4, 2N) - \delta(k_1 + k_2 + k_3, 2N + k_4) \\ & - \delta(k_1 + k_2 + k_4, 2N + k_3) - \delta(k_1 + k_3 + k_4, 2N + k_2) - \delta(k_2 + k_3 + k_4, 2N + k_1), \end{aligned} \quad (6)$$

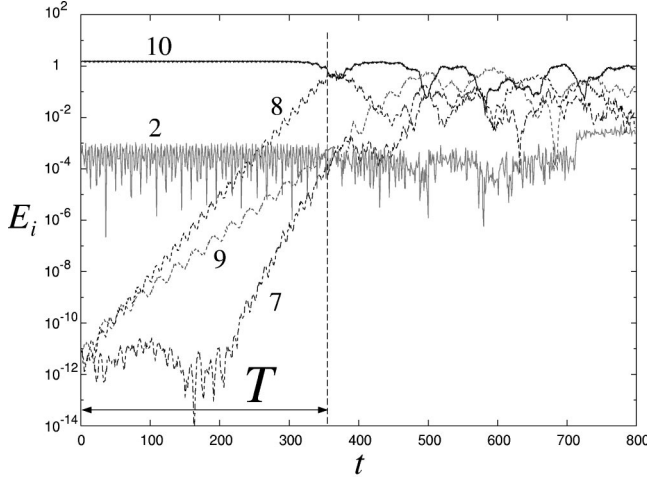


FIG. 1. Mode energies E_i plotted versus time t . $N=16$, $k=10$, and $\epsilon=0.1$.

where δ is the Kronecker delta function. The linear energy E_i of each normal mode is defined as

$$E_i(t) = \frac{1}{2} [P_i^2(t) + \omega_i^2 Q_i^2(t)]. \quad (7)$$

The equation of motion for a normal mode is

$$\frac{d^2}{dt^2} Q_k + \omega_k^2 Q_k + \frac{\beta}{2N} \sum_{k_1, k_2, k_3=1}^{N-1} \omega_k \omega_{k_1} \omega_{k_2} \omega_{k_3} \times Q_{k_1} Q_{k_2} Q_{k_3} D(k, k_1, k_2, k_3) = 0. \quad (8)$$

The initial conditions considered in the present study consist of an almost single-mode excitation: at the initial time, most of the energy is given to a single normal mode of wave number k and only a small amount of energy is placed in the other modes. Thus,

$$Q_i(0) \approx 0, \quad \dot{Q}_i(0) \approx 0 \quad (i \neq k). \quad (9)$$

The nature of these initial conditions implies that $E_i(t) \approx 0$ ($i \neq k$) holds for some period, and then significant energy is transferred from the initially excited mode to others. In this paper, we investigate this process of energy exchange.

III. ENERGY EXCHANGE AND ORBIT INSTABILITY

A. Induction phenomenon

The induction phenomenon was first reported in a numerical study of the energy exchange in the FPU β model [17]. This phenomenon is observed most often in the small energy density regime. We start with a numerical example calculated for the system of $N=16$ and $\beta=1$. The energy density ϵ is set to 0.1 and the mode $k=10$ is initially excited. A small amount of energy (1×10^{-10}) ϵ is initially placed in every other mode. This initial condition allows the odd modes to participate in the energy exchange. Figure 1 shows some of the mode energies E_i plotted versus time t . In an early stage of the time evolution, some of the mode energies E_i ($i \neq k$) grow exponentially. The energies of all the modes except that of mode 10 become large, and significant energy

is transferred from mode 10 to these modes at $t \approx 350$. The period prior to the significant energy exchange is called the induction period and its length the induction time, which we denote by T . The growth rates are different between the modes: mode 8 has the largest growth rate in the early part of the induction period. After the induction period, the energy exchange among the modes seems chaotic. In the present paper, we investigate some properties of the mode dynamics during the induction period and some properties of T .

B. Exponential instability of orbits

In this subsection, we discuss the relationship between the exponential growth of mode energies and the exponential instability of nearby orbits in phase space. The amount of energy in the modes other than the initially excited one is given by

$$\Delta E(t) = \sum_{i \neq k} \frac{1}{2} [P_i^2(t) + \omega_i^2 Q_i^2(t)]. \quad (10)$$

We denote a point in phase space by $\Gamma = (\mathbf{P}, \mathbf{Q})$ and define the norm normal to the plane $\Pi = \{(\mathbf{P}, \mathbf{Q}) | P_i = Q_i = 0, i \neq k\}$ as $\|\Gamma\|_{\perp}^2 = \sum_{i \neq k} (P_i^2 + Q_i^2)$. Due to the initial condition $P_i(0) \approx 0$, $Q_i(0) \approx 0$ ($i \neq k$), the normal norm of $\Gamma(t) - \Gamma(0)$ is approximately given by

$$\|\Gamma(t) - \Gamma(0)\|_{\perp}^2 \approx \sum_{i \neq k} [P_i^2(t) + Q_i^2(t)]. \quad (11)$$

From Eqs. (4), (10), and (11), we have the inequalities

$$\frac{w_1^2}{2} \|\Gamma(t) - \Gamma(0)\|_{\perp}^2 \leq \Delta E(t) \leq \frac{w_{N-1}^2}{2} \|\Gamma(t) - \Gamma(0)\|_{\perp}^2. \quad (12)$$

These can be rewritten as

$$\begin{aligned} & \frac{2}{t} \ln \|\Gamma(t) - \Gamma(0)\|_{\perp} + \frac{1}{t} \ln \frac{w_1^2}{2} \\ & \leq \frac{1}{t} \ln \Delta E(t) \\ & \leq \frac{2}{t} \ln \|\Gamma(t) - \Gamma(0)\|_{\perp} + \frac{1}{t} \ln \frac{w_{N-1}^2}{2}. \end{aligned} \quad (13)$$

For a sufficiently large t , we obtain

$$\frac{1}{t} \ln \Delta E(t) \approx 2 \left[\frac{1}{t} \ln \|\Gamma(t) - \Gamma(0)\|_{\perp} \right]. \quad (14)$$

This indicates that the exponential growth rate of ΔE is twice as large as that of the phase point separation from the initial point.

Figure 2 shows the phase point separation. Let $\Gamma(t; S_0)$ be a solution that has an initial point S_0 at $t=0$. Since an almost single-mode excitation is employed as initial condition, an almost single-mode oscillation of the initially excited mode lasts during the induction period, and thus the phase point returns to the neighborhood of the initial point after the single-mode oscillation period t_0 . The points S_n (n

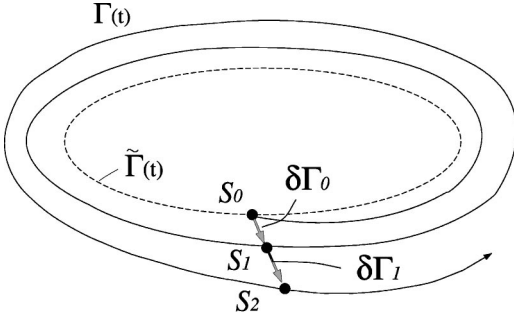


FIG. 2. Schematic illustration of an orbit in phase space. The solid curve represents the actual orbit and the dashed curve the pseudoperiodic orbit.

$=1, 2, \dots$) represent the phase points $\Gamma(nt_0; S_0)$, which are close to S_0 . Defining $\delta\Gamma_i = \Gamma((i+1)t_0; S_0) - \Gamma(it_0; S_0)$, we have

$$\Gamma(nt_0) - \Gamma(0) = \sum_{i=0}^{n-1} \delta\Gamma_i. \quad (15)$$

Consider an orbit $\Gamma(t; S_1)$ that has the initial point S_1 at $t=0$, i.e., $\Gamma(t; S_1) = \Gamma(t+t_0; S_0)$. Since S_1 is close to the initial point S_0 , the time evolution of the difference $\Gamma(t; S_1) - \Gamma(t; S_0)$ can be approximately described by the variational equation

$$\begin{aligned} \frac{d^2}{dt^2} \xi_i + \omega_i^2 \xi_i + \frac{3\beta}{2N} \sum_{j, k_1, k_2=1}^{N-1} \omega_i \omega_j \omega_{k_1} \omega_{k_2} \\ \times Q_{k_1}(t) Q_{k_2}(t) \xi_j D(i, j, k_1, k_2) = 0, \end{aligned} \quad (16)$$

where ξ_i ($i=1, \dots, N-1$) represents the variation in the normal mode coordinate Q_i and $Q_{k_1, k_2}(t)$ a component of the reference orbit $\Gamma(t; S_0)$. Equation (16) is obtained by linearizing Eq. (8) along the reference orbit. The solution $\xi = (\xi_1, \dots, \xi_{N-1}, \xi_1, \dots, \xi_{N-1})$ of Eq. (16) with the initial condition $\xi(0) = \delta\Gamma_0$ can approximate the time evolution of the difference $\Gamma(t; S_1) - \Gamma(t; S_0)$. Therefore, we have the approximate expression

$$\Gamma(nt_0) - \Gamma(0) \approx \sum_{i=0}^{n-1} \xi(it_0). \quad (17)$$

C. Average variational equation

In this subsection, we introduce an approximate version of the variational equation (16) as a tool for our theoretical analysis; we call this an *average variational equation* (AVE). Since we are interested in the mode dynamics over the induction period, the exponential growth rate of ξ in the period $t < T$ (rather than through infinite time) is useful. The initially excited mode has the only significant amplitude since the amplitudes of the other modes are sufficiently small during the induction period. This fact enables us to simplify the variational equation (16).

If the approximation $Q_i(t) = 0$ ($i \neq k$) is made in Eq. (8), the equation of motion for the k th mode (the mode excited initially) is approximated as

$$\frac{d^2}{dt^2} Q_k + \omega_k^2 Q_k + \frac{3\beta}{2N} \omega_k^4 Q_k^3 = 0. \quad (18)$$

It is well known that the solution of Eq. (18) may be written, with the Jacobi elliptic function, in the form

$$\tilde{Q}_k(t) = a \sqrt{N} \text{cn}(\sigma t, k_m), \quad (19)$$

where

$$a^2 = \frac{4k_m^2}{3\beta\omega_k^2(1-2k_m^2)}, \quad \sigma^2 = \frac{\omega_k^2}{1-2k_m^2}, \quad (20)$$

and k_m is the modulus of the Jacobi elliptic function. The modulus k_m is related to the energy density ϵ as

$$\epsilon = \frac{2k_m^2(1-k_m^2)}{3\beta(1-2k_m^2)^2}. \quad (21)$$

In phase space, the solution $\tilde{Q}_k(t)$ defines the periodic orbit $\tilde{\Gamma}(t)$ whose nonzero components are only the k th momentum \tilde{P}_k and amplitude \tilde{Q}_k . Since $\tilde{Q}_k(t)$ is an approximate rather than an exact solution, the periodic orbit $\tilde{\Gamma}(t)$ is also only approximate. In this sense, we call $\tilde{\Gamma}(t)$ a *pseudoperiodic orbit*. An orbit starting with an almost single-mode excitation initial condition remains close to the pseudoperiodic orbit for $t < T$ (see Fig. 2). In other words, the pseudoperiodic orbit approximates, in an average sense, the actual orbit generated by the equations of motion (8) for $t < T$. Therefore, we replace the reference orbit in Eq. (16) with the pseudoperiodic orbit \tilde{Q}_k . That is, the variational equation employed for the theoretical analysis is

$$\frac{d^2}{dt^2} \xi_i + \omega_i^2 \xi_i + \frac{3\beta}{2N} \omega_k^2 \tilde{Q}_k^2(t) \sum_{j=1}^{N-1} \omega_i \omega_j \xi_j D(i, j, k, k) = 0. \quad (22)$$

The actual reference orbit may contain a small oscillating part other than \tilde{Q}_k . This small oscillating part might affect the growth of the solution. However, we first assume that only the contribution of \tilde{Q}_k is important and later confirm that this assumption is acceptable by comparing the theoretical results with numerical results.

Since \tilde{Q}_k is a periodic function, the AVE is a so-called *coupled Hill equation*. We denote the period of \tilde{Q}_k by t_0 . According to Floquet theory, solutions of Eq. (22) at $t=0$ and t_0 are related via the *monodromy matrix* M as $\xi(t_0) = M\xi(0)$. The AVE is a Hamiltonian system itself with the Hamiltonian

$$\begin{aligned} H_{AVE} = \frac{1}{2} \sum_{i=1}^{N-1} (\xi_i^2 + \omega_i^2 \xi_i^2) \\ + \frac{3\beta}{4N} \omega_k^2 \tilde{Q}_k^2(t) \sum_{i,j=1}^{N-1} \omega_i \omega_j \xi_i \xi_j D(i, j, k, k). \end{aligned} \quad (23)$$

Let $\alpha_i \in \mathbb{C}[i=1, \dots, 2(N-1); |\alpha_1| \geq \dots \geq |\alpha_{2(N-1)}|]$ be eigenvalues of the monodromy matrix M of the AVE. Because of simplicity of the AVE, the eigenvalues satisfy the relations $\alpha_{2(N-1)} = \alpha_1^{-1}, \dots, \alpha_N = \alpha_{N-1}^{-1}$. Therefore, if $|\alpha_1| = 1$, all of the eigenvalues are on the unit circle of the complex plane, i.e., $|\alpha_1| = \dots = |\alpha_{2(N-1)}| = 1$.

If we approximate the variational vector ξ in Eq. (17) using the solution of the AVE, we have

$$\Gamma(nt_0) - \Gamma(0) \simeq \sum_{i=0}^{n-1} M^i \xi(0). \quad (24)$$

Let α_{i_j} ($j=1, \dots, d; |\alpha_{i_1}| \geq \dots \geq |\alpha_{i_d}|$) be distinct eigenvalues of M , where $i_1=1$ and $P^{(i_j)}$ is a projection onto the eigenspace of α_{i_j} . Since some eigenvalues may have the same modulus as α_{i_1} , we assume $|\alpha_{i_1}| = \dots = |\alpha_{i_s}|$ ($s \leq d$). We consider a simple case where the monodromy matrix M is diagonalizable. The monodromy matrix M can be written as

$$M = \alpha_{i_1} P^{(i_1)} + \dots + \alpha_{i_d} P^{(i_d)}. \quad (25)$$

Substituting this into Eq. (24) and assuming that $\alpha_{i_j} \neq 1$ ($j=1, \dots, d$), we obtain

$$\begin{aligned} \|\Gamma(nt_0) - \Gamma(0)\| & \simeq \left\| \left[\sum_{i=0}^{n-1} \alpha_{i_1}^i P^{(i_1)} + \dots + \sum_{i=0}^{n-1} \alpha_{i_d}^i P^{(i_d)} \right] \xi(0) \right\| \\ & = \left\| \sum_{j=1}^d \left(\frac{\alpha_{i_j}^n - 1}{\alpha_{i_j} - 1} \right) P^{(i_j)} \xi(0) \right\|. \end{aligned} \quad (26)$$

It is generally expected that $P^{(i_j)} \xi(0) \neq \mathbf{0}$ ($j=1, \dots, s$) and these terms become dominant for large n in the case of $|\alpha_1| > 1$. (Precisely speaking, the terms that correspond to the eigenvalues with moduli close to $|\alpha_1|$ are also important for finite n .) Therefore, we can obtain the scaling

$$\|\Gamma(nt_0) - \Gamma(0)\| \sim |\alpha_1|^n = \exp(\lambda_1 nt_0), \quad (27)$$

where we defined the largest characteristic exponent (LCE) λ_1 as $\lambda_1 = \ln|\alpha_1|/t_0$. Since $\Gamma(nt_0) - \Gamma(0)$ may contain a component normal to the plane Π , the normal norm $\|\Gamma(nt_0) - \Gamma(0)\|_{\perp}$ also follows the same scaling law. From Eq. (14), the growth of $\Delta E(t)$ is approximated as

$$\Delta E(t) \simeq \Delta E_0 \exp(2\lambda_1 t), \quad (28)$$

where ΔE_0 represents the value of $\Delta E(t)$ at the initial stage $t = O(t_0)$. The induction time T can be estimated as the time at which ΔE becomes of the same order as the total energy E , i.e., $\Delta E(T) = O(E)$. Therefore, we can estimate T as

$$T \simeq \frac{1}{2\lambda_1} \ln \frac{E}{\Delta E_0}. \quad (29)$$

This shows that T can be estimated by using the inverse of λ_1 since the dependence on the logarithmic factor is expected to be weak.

We proceed to the case of $|\alpha_1| = 1$ and $\alpha_{i_j} \neq 1$ ($j=1, \dots, d$). In this case, all the eigenvalues are on the unit circle ($|\alpha_1| = \dots = |\alpha_{2(N-1)}| = 1$), so the right hand side of Eq. (26) is bounded as

$$\left\| \sum_{j=1}^d \left(\frac{\alpha_{i_j}^n - 1}{\alpha_{i_j} - 1} \right) P^{(i_j)} \xi(0) \right\| \leq \sum_{j=1}^d \frac{2}{|\alpha_{i_j} - 1|} \|P^{(i_j)} \xi(0)\|. \quad (30)$$

We evaluate the order of the right hand side in Eq. (30) for a sufficiently small ϵ . In the limit $\epsilon \rightarrow 0$, the equations of motion (8) reduce to those of harmonic oscillators, and the AVE also reduces to the equation for $\beta = 0$. The eigenvalues of M are given by $e^{\pm i2\pi\omega_1/\omega_k}, \dots, e^{\pm i2\pi\omega_{N-1}/\omega_k}$, since the period is $t_0 = 2\pi/\omega_k$. If we assume the initial condition $\Gamma(0)$ as $P_i(0) = \omega_i \rho_i \cos \psi_i$, $Q_i(0) = \rho_i \sin \psi_i$ ($i=1, \dots, N-1$), where $|\rho_i| \ll |\rho_k|$ ($i \neq k$), we can calculate the right hand side in this limit as

$$\sum_{j=1}^d \frac{2}{|\alpha_{i_j} - 1|} \|P^{(i_j)} \xi(0)\| = 2 \sum_{\substack{i=1 \\ i \neq k}}^{N-1} \rho_i \sqrt{1 + \omega_i^2}, \quad (31)$$

$$\leq 2\sqrt{5} \sum_{\substack{i=1 \\ i \neq k}}^{N-1} \rho_i. \quad (32)$$

Since the right hand side of Eq. (30) is a continuous function of ϵ , it is still of the order of $O(\sum_{i \neq k} \rho_i)$ for sufficiently small ϵ . This shows that the right hand side is small if the initial amplitudes ρ_i of the modes other than the dominant mode k are sufficiently small. Therefore, Eq. (30) shows that within the AVE approximation, the phase point separation $\Gamma(nt_0) - \Gamma(0)$ does not significantly increase but is bounded by a small value. This implies that every E_i of the modes other than the initially excited one remains of the order of its value at the initial stage, and thus the induction time T diverges when ϵ is sufficiently small and $|\alpha_1| = 1$ (or $\lambda_1 = 0$).

IV. ANALYTICAL COMPUTATION OF THE LCE

In this section, we carry out an analytical computation of the LCE. For this purpose, we introduce a further approximation to the AVE and then apply the second order averaging method.

A. Averaging method

We briefly review the averaging method [21] in this subsection. The averaging method is applicable to an equation of the standard form,

$$\frac{dx}{dt} = \gamma F(x, t), \quad (33)$$

where $x \in \mathbf{R}^n$, $t \in \mathbf{R}$, and γ is a small parameter. We assume that the function $F(x, t)$ is periodic in t and takes the form

$$F(x, t) = \sum_{\nu=-\infty}^{\infty} F^{(\nu)}(x) e^{i\nu\omega t}. \quad (34)$$

We introduce the following two operators $M_i\{\mathbf{F}\}$ and $\bar{\mathbf{F}}$:

$$M_i\{\mathbf{F}(\mathbf{x}, t)\} = \mathbf{F}^{(0)}(\mathbf{x}), \quad (35)$$

$$\bar{\mathbf{F}}(\mathbf{x}, t) = \sum_{\nu \neq 0} \frac{1}{i\nu\omega} \mathbf{F}^{(\nu)}(\mathbf{x}) e^{i\nu\omega t}. \quad (36)$$

Since the parameter γ is assumed to be sufficiently small, it is reasonable to expect that the solution \mathbf{x} to Eq. (33) varies very slowly and a fast variation of \mathbf{F} in t does not cause a significant variation of \mathbf{x} . Therefore, the averaging method approximates Eq. (33) by using an *averaged autonomous equation*. The first order averaged equation is given by

$$\frac{d\mathbf{x}_0}{dt} = \gamma M_i\{\mathbf{F}(\mathbf{x}_0, t)\}. \quad (37)$$

The solution \mathbf{x} of Eq. (33) can be approximated to first order with the solution \mathbf{x}_0 of Eq. (37), namely, $\mathbf{x} = \mathbf{x}_0$.

As we will mention later, the first order averaged solution turns out to be inadequate for appropriately computing the LCE. Therefore, we use a second order averaging method in this study. To second order, the averaged equation is given by

$$\frac{d\mathbf{x}_0}{dt} = \gamma M_i\{\mathbf{F}(\mathbf{x}_0, t)\} + \gamma^2 M_i\left\{\left(\bar{\mathbf{F}} \cdot \frac{\partial}{\partial \mathbf{x}_0}\right) \mathbf{F}(\mathbf{x}_0, t)\right\}. \quad (38)$$

The operator $\bar{\mathbf{F}} \cdot \partial / \partial \mathbf{x}_0$ is defined by

$$\bar{\mathbf{F}} \cdot \frac{\partial}{\partial \mathbf{x}_0} = \sum_{j=1}^n \bar{F}_j(\mathbf{x}_0, t) \frac{\partial}{\partial x_{0j}}, \quad (39)$$

where \bar{F}_j and x_{0j} represent components of $\bar{\mathbf{F}}$ and \mathbf{x}_0 , respectively. The solution \mathbf{x} can be approximated to the second order as $\mathbf{x} = \mathbf{x}_0 + \gamma \bar{\mathbf{F}}(\mathbf{x}_0, t)$.

B. Two-mode approximation of the AVE

It is difficult to analyze the stability of solutions to Eq. (22) directly because of the high dimensionality, except for the simple case where Eq. (22) separates into $N-1$ decoupled equations. A stability analysis in such a simple case was carried out in [22,23]. In order to overcome this difficulty, we attempt to approximate the AVE by using a low-dimensional equation consisting of a few important mode components. In our previous work [8], we showed that for a sufficiently large energy density parametric resonance among four specific mode components is dominant for the instability and the AVE can be well approximated with a four-dimensional equation including only the couplings among these four modes. The energy density range for the induction phenomenon is smaller than this. Therefore, in this study, we deal with the AVE in a smaller energy density regime and the dominant mode couplings in the AVE are different.

We numerically integrate Eq. (22) and calculate the variational vectors that correspond to some of the largest characteristic exponents, in order to find a set of a small number of important mode components. We started the numerical integration with six different initial conditions and converged the

variational vectors to those giving the six largest characteristic exponents by iteratively orthonormalizing them. Figures 3(a)–3(f) show $\xi_i^2 + \xi_i'^2$ of those vectors plotted against i for λ_1 – λ_6 , respectively. In the numerical calculation, we set the parameters as $N=64$, $k=43$, $\beta=1$, and $\epsilon=0.01$. The AVE appears to have multiple characteristic exponents, i.e., $\lambda_1 = \lambda_2$, $\lambda_3 = \lambda_4$, and $\lambda_5 = \lambda_6$, or equivalently, $|\alpha_1| = |\alpha_2|$, $|\alpha_3| = |\alpha_4|$, and $|\alpha_5| = |\alpha_6|$.

The figures show that only two components have non-negligible values and the others are almost equal to zero. These two components have mode numbers $k \pm m$, where m is a positive integer. The two non-negligible components are 43 ± 3 for λ_1 and λ_2 , 43 ± 4 for λ_3 and λ_4 , and 43 ± 2 for λ_5 and λ_6 . Based on this numerical observation, we assume that the parametric resonance between the $k-m$ and $k+m$ mode components is dominant for the instability in the AVE. The importance of such a coupling was also pointed out in [24]. If we retain only the two-mode components of $k \pm m$ in Eq. (22), then we have equations of the form

$$\begin{aligned} \frac{d^2}{dt^2} \xi_{i_1} + \omega_{i_1}^2 \xi_{i_1} + \frac{3\beta}{2N} \omega_k^2 \tilde{Q}_k^2(t) \\ \times (2\omega_{i_1}^2 \xi_{i_1} + \omega_{i_1} \omega_{i_2} \xi_{i_2}) = 0, \end{aligned} \quad (40)$$

$$\begin{aligned} \frac{d^2}{dt^2} \xi_{i_2} + \omega_{i_2}^2 \xi_{i_2} + \frac{3\beta}{2N} \omega_k^2 \tilde{Q}_k^2(t) \\ \times (\omega_{i_1} \omega_{i_2} \xi_{i_1} + 2\omega_{i_2}^2 \xi_{i_2}) = 0, \end{aligned}$$

where i_1 and i_2 stand for $k-m$ and $k+m$, respectively. This type of coupling between modes $k \pm m$ exists for the initial excitation of any mode k except $k=1$, $N/2$, and $N-1$: the modes $k=1$ and $N-1$ do not have one of the pair $k \pm m$ since they are the boundary modes, and for $k=N/2$ the AVE separates into $N-1$ decoupled equations. Therefore, the following theoretical analysis applies to the case of any k except $k=1$, $N/2$, and $N-1$.

We solve this set of equations for any m and calculate its two positive characteristic exponents as a function of m . From the above numerical observation, we can assume that a pair of positive characteristic exponents for a single m gives some successive characteristic exponents λ_{2j-1} and λ_{2j} , where $j=1, 2, \dots$. In other words, letting W_{2j-1} and W_{2j} be the eigenspaces of α_{2j-1} and α_{2j} , respectively, we can assume that the real subspace of their direct sum, $(W_{2j-1} \oplus W_{2j}) \cap \mathbf{R}^{2(N-1)}$, is approximately included in a four-dimensional subspace $U_{k \pm m} = \{(\mathbf{P}, \mathbf{Q}) | P_i = Q_i = 0, i \neq k \pm m\}$ of phase space, which is spanned by the two mode components $k \pm m$. Next, we look for the m that gives the maximum of those m -dependent characteristic exponents in order to determine the LCE λ_1 .

If we introduce a new time variable $\tau = \omega_k t$ and rewrite the dependent variables with $\zeta_1 = \xi_{i_1}$ and $\zeta_2 = \xi_{i_2}$ in Eqs. (40), then we obtain the equations

$$\frac{d^2}{d\tau^2} \zeta_1 + r_1^2 \zeta_1 + \frac{3}{2} \beta \phi^2(\tau) (2r_1^2 \zeta_1 + r_1 r_2 \zeta_2) = 0, \quad (41)$$

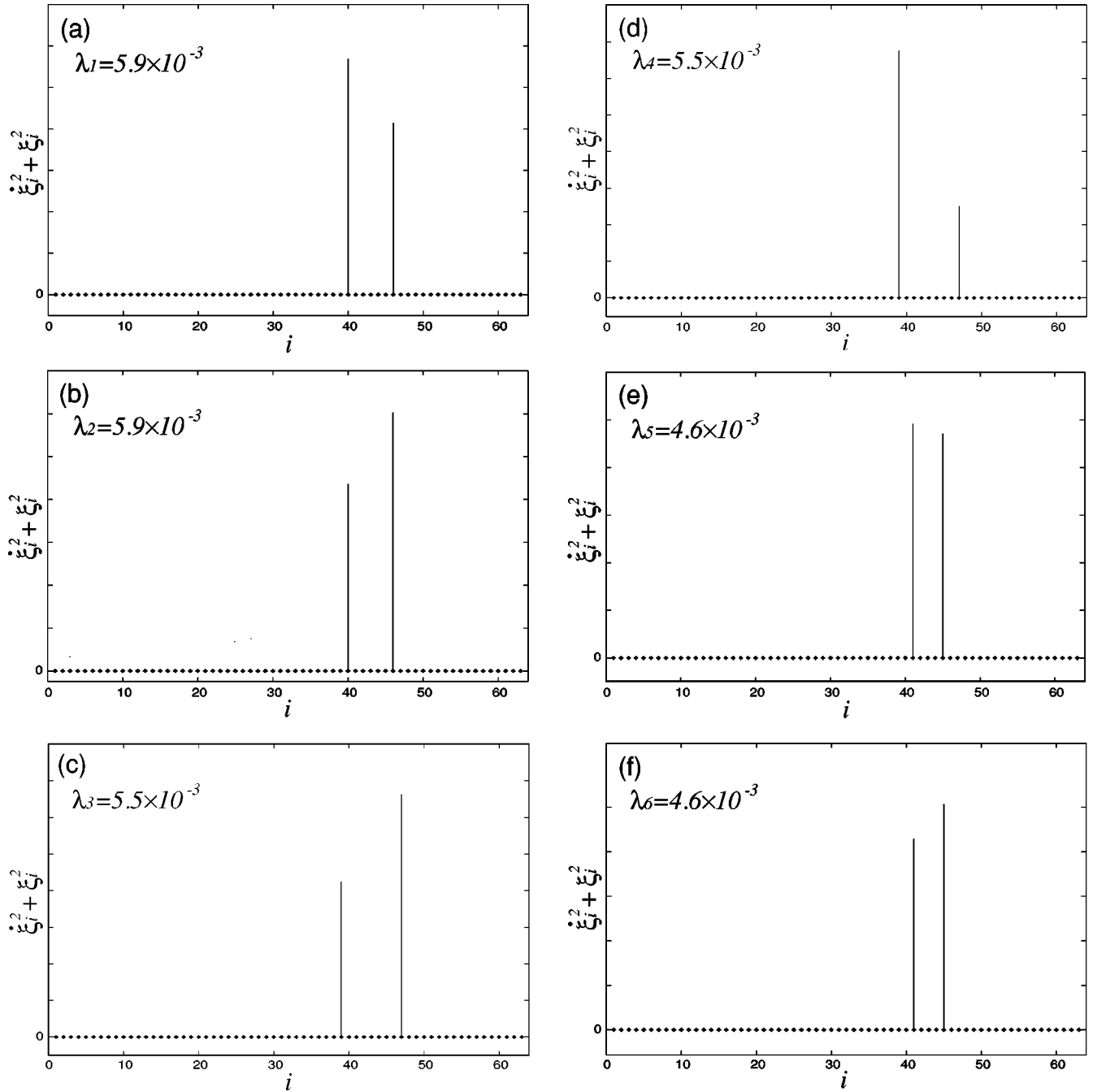


FIG. 3. Variational vectors corresponding to the six largest characteristic exponents calculated for $N=64$, $k=43$, and $\epsilon=0.01$. $\xi_i^2 + \xi_j^2$ is plotted against i . (a) $\lambda_1=5.9 \times 10^{-3}$. (b) $\lambda_2=5.9 \times 10^{-3}$. (c) $\lambda_3=5.5 \times 10^{-3}$. (d) $\lambda_4=5.5 \times 10^{-3}$. (e) $\lambda_5=4.6 \times 10^{-3}$. (f) $\lambda_6=4.6 \times 10^{-3}$.

$$\frac{d^2}{d\tau^2} \zeta_2 + r_2^2 \zeta_2 + \frac{3}{2} \beta \phi^2(\tau) (r_1 r_2 \zeta_1 + 2r_2^2 \zeta_2) = 0,$$

where r_1 and r_2 are the ratios between two frequencies defined by

$$r_1 = \frac{\omega_{i_1}}{\omega_k} = \frac{\sin[\pi(k-m)/2N]}{\sin(\pi k/2N)},$$

$$r_2 = \frac{\omega_{i_2}}{\omega_k} = \frac{\sin[\pi(k+m)/2N]}{\sin(\pi k/2N)},$$
(42)

and the function $\phi(\tau)$ is defined as

$$\phi(\tau) = \frac{\omega_k}{\sqrt{N}} \tilde{Q}_k(\tau/\omega_k) = A \operatorname{cn}[(1+6\beta\epsilon)^{1/4} \tau, k_m],$$
(43)

where k_m is the modulus defined in Eq. (21) and the amplitude A is given by

$$A^2 = \frac{2}{3\beta} (-1 + \sqrt{1+6\beta\epsilon}).$$
(44)

Note that the function ϕ depends on neither k nor N .

C. Application of averaging method

We solve Eqs. (41) for small ϵ using the second order averaging method. From Eq. (43), the period of the function ϕ is given by

$$\tau_0 = \frac{4K(k_m)}{(1+6\beta\epsilon)^{1/4}} = \frac{4}{(1+6\beta\epsilon)^{1/4}} \int_0^{\pi/2} \frac{d\theta}{\sqrt{1-k_m^2 \sin^2 \theta}}, \quad (45)$$

where $K(k_m)$ represents the elliptic integral with modulus k_m defined in Eq. (21). The corresponding angular frequency is

$$\Omega = \frac{2\pi}{\tau_0} = \frac{\pi(1+6\beta\epsilon)^{1/4}}{2K(k_m)}. \quad (46)$$

Using the approximation $\phi(\tau) = A \cos(\Omega\tau)$, we bring Eqs. (41) to the form

$$\frac{d^2}{d\tau^2} \zeta_1 + r_1^2 \zeta_1 + \gamma[1 + \cos(2\Omega\tau)](2r_1^2 \zeta_1 + r_1 r_2 \zeta_2) = 0, \quad (47)$$

$$\frac{d^2}{d\tau^2} \zeta_2 + r_2^2 \zeta_2 + \gamma[1 + \cos(2\Omega\tau)](r_1 r_2 \zeta_1 + 2r_2^2 \zeta_2) = 0,$$

where the small parameter γ is defined by $\gamma = (3/4)\beta A^2$. We assume a solution to Eqs. (47) in the form

$$\zeta_i = u_i(\tau) \sin(\Omega\tau) + v_i(\tau) \cos(\Omega\tau), \quad (48)$$

$$\frac{d\zeta_i}{d\tau} = \Omega u_i(\tau) \cos(\Omega\tau) - \Omega v_i(\tau) \sin(\Omega\tau), \quad (49)$$

where $i = 1, 2$. If we substitute Eqs. (48) and (49), then Eqs. (47) are rewritten in the form

$$\begin{aligned} \frac{du_1}{d\tau} &= \frac{\gamma}{\Omega} \left[\left(\frac{1}{2} a_{13} v_1 - \frac{3}{4} b_{12} v_2 \right) + \left(\frac{1}{2} a_{12} u_1 - \frac{1}{2} b_{12} u_2 \right) \sin(2\Omega\tau) + \left(\frac{1}{2} a_{14} v_1 - b_{12} v_2 \right) \cos(2\Omega\tau) \right. \\ &\quad \left. + \left(-\frac{1}{2} b_{11} u_1 - \frac{1}{4} b_{12} u_2 \right) \sin(4\Omega\tau) + \left(-\frac{1}{2} b_{11} v_1 - \frac{1}{4} b_{12} v_2 \right) \cos(4\Omega\tau) \right], \\ \frac{dv_1}{d\tau} &= \frac{\gamma}{\Omega} \left[\left(-\frac{1}{2} a_{11} u_1 + \frac{1}{4} b_{12} u_2 \right) + \left(-\frac{1}{2} a_{12} v_1 + \frac{1}{2} b_{12} v_2 \right) \sin(2\Omega\tau) + \left(\frac{1}{2} a_{10} u_1 \right) \cos(2\Omega\tau) \right. \\ &\quad \left. + \left(\frac{1}{2} b_{11} v_1 + \frac{1}{4} b_{12} v_2 \right) \sin(4\Omega\tau) + \left(-\frac{1}{2} b_{11} u_1 - \frac{1}{4} b_{12} u_2 \right) \cos(4\Omega\tau) \right], \end{aligned} \quad (50)$$

$$\begin{aligned} \frac{du_2}{d\tau} &= \frac{\gamma}{\Omega} \left[\left(\frac{1}{2} a_{23} v_2 - \frac{3}{4} b_{21} v_1 \right) + \left(\frac{1}{2} a_{22} u_2 - \frac{1}{2} b_{21} u_1 \right) \sin(2\Omega\tau) + \left(\frac{1}{2} a_{24} v_2 - b_{21} v_1 \right) \cos(2\Omega\tau) \right. \\ &\quad \left. + \left(-\frac{1}{2} b_{22} u_2 - \frac{1}{4} b_{21} u_1 \right) \sin(4\Omega\tau) + \left(-\frac{1}{2} b_{22} v_2 - \frac{1}{4} b_{21} v_1 \right) \cos(4\Omega\tau) \right], \end{aligned}$$

$$\begin{aligned} \frac{dv_2}{d\tau} &= \frac{\gamma}{\Omega} \left[\left(-\frac{1}{2} a_{21} u_2 + \frac{1}{4} b_{21} u_1 \right) + \left(-\frac{1}{2} a_{22} v_2 + \frac{1}{2} b_{21} v_1 \right) \sin(2\Omega\tau) + \left(\frac{1}{2} a_{20} u_2 \right) \cos(2\Omega\tau) \right. \\ &\quad \left. + \left(\frac{1}{2} b_{22} v_2 + \frac{1}{4} b_{21} v_1 \right) \sin(4\Omega\tau) + \left(-\frac{1}{2} b_{22} u_2 - \frac{1}{4} b_{21} u_1 \right) \cos(4\Omega\tau) \right], \end{aligned}$$

where we defined the coefficients a_{ij} and b_{ij} as

$$a_{ij} = \frac{1}{\gamma} [\Omega^2 - r_i^2 (1 + j\gamma)], \quad (51)$$

$$b_{ij} = r_i r_j. \quad (52)$$

We assume that m/N is much smaller than k/N in the present analysis. This assumption guarantees that $r_1 \approx 1$ and $r_2 \approx 1$. In addition, we can see that $\Omega \approx 1$ if ϵ is sufficiently small. Since these imply $a_{ij} \ll O(\gamma^{-1})$ and $b_{ij} = O(1)$, Eqs. (50) are in the standard form (33); thus, the averaging method is applicable when $m/N \ll k/N$ and $\epsilon \ll 1$.

If we calculate the second order averaged equations according to Eq. (38), then we arrive at equations of the form

$$\frac{d}{d\tau} \begin{pmatrix} u_1 \\ v_1 \\ u_2 \\ v_2 \end{pmatrix} = \frac{\gamma}{4\Omega} \begin{pmatrix} 0 & 2\Delta_{1u} & 0 & -3R_1 \\ -2\Delta_{1v} & 0 & R_2 & 0 \\ 0 & -3R_1 & 0 & 2\Delta_{2u} \\ R_2 & 0 & -2\Delta_{2v} & 0 \end{pmatrix} \times \begin{pmatrix} u_1 \\ v_1 \\ u_2 \\ v_2 \end{pmatrix}, \quad (53)$$

where the matrix elements $\Delta_{1u}, \Delta_{1v}, \Delta_{2u}, \Delta_{2v}, R_1,$ and $R_2,$ respectively, are defined as

$$\Delta_{1u} = a_{13} + \frac{\gamma}{32\Omega^2} (8a_{12}a_{14} + 4b_{11}^2 + 17b_{12}^2), \quad (54)$$

$$\Delta_{1v} = a_{11} + \frac{\gamma}{32\Omega^2} (8a_{10}a_{12} + 4b_{11}^2 + b_{12}^2), \quad (55)$$

$$\Delta_{2u} = a_{23} + \frac{\gamma}{32\Omega^2} (8a_{22}a_{24} + 4b_{22}^2 + 17b_{12}^2), \quad (56)$$

$$\Delta_{2v} = a_{21} + \frac{\gamma}{32\Omega^2} (8a_{20}a_{22} + 4b_{22}^2 + b_{12}^2), \quad (57)$$

$$R_1 = b_{12} + \frac{\gamma}{48\Omega^2} [4b_{12}(2a_{12} + a_{14} + a_{24} + 2a_{22}) - 2b_{12}(b_{11} + b_{22})], \quad (58)$$

$$R_2 = b_{12} + \frac{\gamma}{16\Omega^2} [4b_{12}(a_{10} + a_{20}) - 2b_{12}(b_{11} + b_{22})]. \quad (59)$$

The eigenvalues λ of the coefficient matrix in Eq. (53) can be explicitly obtained as

$$\lambda = \pm \frac{\gamma}{4\Omega} [-3R_1R_2 - 2(\Delta_{1u}\Delta_{1v} + \Delta_{2u}\Delta_{2v}) \pm 2\{(\Delta_{1u}R_2 + 3\Delta_{2v}R_1)(\Delta_{2u}R_2 + 3\Delta_{1v}R_1) + (\Delta_{1u}\Delta_{1v} - \Delta_{2u}\Delta_{2v})^2\}^{1/2}]^{1/2}. \quad (60)$$

We write the polynomials in Eq. (60) as

$$F = (\Delta_{1u}R_2 + 3\Delta_{2v}R_1)(\Delta_{2u}R_2 + 3\Delta_{1v}R_1) + (\Delta_{1u}\Delta_{1v} - \Delta_{2u}\Delta_{2v})^2, \quad (61)$$

$$G = -3R_1R_2 - 2(\Delta_{1u}\Delta_{1v} + \Delta_{2u}\Delta_{2v}). \quad (62)$$

The polynomials F and G depend on ϵ . Calculating them as a function of ϵ , we can see that for fixed m/N and k/N , F

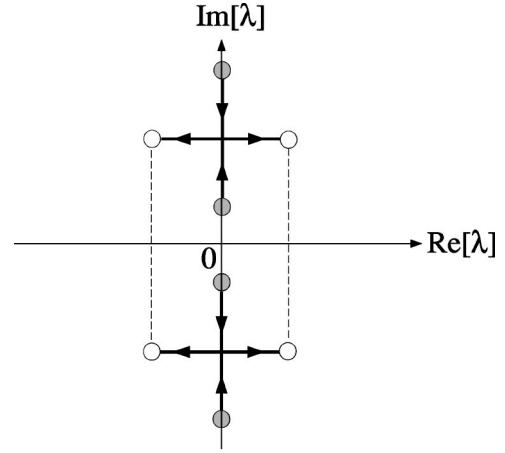


FIG. 4. Diagram for changes in four eigenvalues with ϵ .

changes its sign from positive to negative with an increase in ϵ while G remains negative. Moreover, we can see that $|G|$ is much larger than $|F|$. All the eigenvalues λ are purely imaginary numbers when F is positive. In this case, the solution of Eq. (53) is stable. On the other hand, the four eigenvalues are in the form $\pm(x \pm iy)$ ($x, y \in \mathbf{R}$) when F is negative. Since the positive real parts of two eigenvalues are the same, this coincides with the previous numerical observation indicating that the AVE appears to have multiple characteristic exponents. Figure 4 shows changes in the four eigenvalues in the complex plane with increasing ϵ . When F is negative, the solution of Eq. (53) is unstable and grows at the rate $\text{Re}[\lambda]$, which represents the positive real part of the eigenvalues. The exponential growth rate of a solution (ζ_1, ζ_2) to Eqs. (47) is also given by $\text{Re}[\lambda]$ since terms corresponding to \bar{F} in the second order solution's expression $x = x_0 + \gamma \bar{F}(x_0, t)$ are linear with respect to u_i and v_i .

We proceed to expand $\text{Re}[\lambda]$ in powers of ϵ and m . When $F < 0$, the positive real part of λ is written as

$$\text{Re}[\lambda] = \frac{\gamma}{4\sqrt{2}\Omega} [G + (G^2 + 4|F|)^{1/2}]^{1/2}. \quad (63)$$

If we consider the case of $-F \ll 1$, then $\text{Re}[\lambda]$ can be expanded as

$$\text{Re}[\lambda] \approx \frac{\gamma}{4\Omega} \left(\frac{F}{G} \right)^{1/2}. \quad (64)$$

From Eq. (46), the frequency Ω can be expanded in powers of ϵ as

$$\Omega = 1 + \Omega_1\beta\epsilon + \Omega_2(\beta\epsilon)^2 + O(\epsilon^3) \quad (65)$$

$$= 1 + \frac{9}{8}\beta\epsilon - \frac{621}{256}(\beta\epsilon)^2 + O(\epsilon^3), \quad (66)$$

and, using Eq. (44), we can expand the parameter γ as

$$\gamma = \frac{3}{2}\beta\epsilon - \frac{9}{4}(\beta\epsilon)^2 + O(\epsilon^3). \quad (67)$$

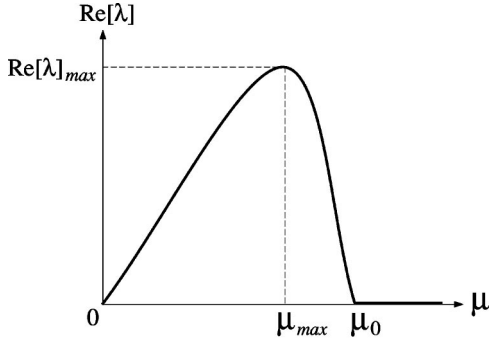


FIG. 5. Illustration of $\text{Re}[\lambda]$ as a function of μ for a fixed ϵ .

We introduce a parameter $\mu = \pi m/2N$, which is small because we assumed a small m/N . Thus, r_i ($i=1,2$) can be expanded by μ . Using the expansions for Ω , γ , and r_i and expanding Eq. (64) to the lowest order of ϵ and μ , we arrive at the following expression:

$$\text{Re}[\lambda] \approx \frac{1}{4} [-4\mu^2\{\mu^2 + 2(2\Omega_1 - 3)\beta\epsilon\}]^{1/2} \quad (68)$$

$$= \frac{1}{4} [-2\mu^2(2\mu^2 - 3\beta\epsilon)]^{1/2}. \quad (69)$$

The expansion coefficient Ω_1 appears in Eq. (68). This shows that the frequency shift of the initially excited mode due to the nonlinearity affects $\text{Re}[\lambda]$ in the lowest order. Figure 5 shows the shape of $\text{Re}[\lambda]$ as a function of μ for a fixed ϵ . The real part $\text{Re}[\lambda]$ is positive for $\mu < \mu_0$ and has a maximum $\text{Re}[\lambda]_{\max}$ at $\mu = \mu_{\max}$. For $\mu > \mu_0$, F is positive, so $\text{Re}[\lambda] = 0$. We can easily find

$$\mu_{\max} = \frac{1}{2} \sqrt{3\beta\epsilon} \quad (70)$$

and the maximum

$$\text{Re}[\lambda]_{\max} = \frac{3}{8} \beta\epsilon. \quad (71)$$

Equation (70) shows that the pair of modes giving $\text{Re}[\lambda]_{\max}$ changes with ϵ : these modes separate from the initially excited one in k space with increasing ϵ and, for large N , their mode numbers k_{\max} are given by

$$k_{\max} = k \pm \left[\frac{N}{\pi} \sqrt{3\beta\epsilon} \right], \quad (72)$$

where $[\cdot]$ on the right hand side means the nearest integer. The mode energies $E_{k_{\max}}$ of these two modes exhibit the largest growth rate.

The maximum $\text{Re}[\lambda]_{\max}$ corresponds to the LCE since the spacing between the neighboring two modes is dense in k/N space and a value sufficiently close to μ_{\max} is possible for large N . As we introduced a new time $\tau = \omega_k t$, the LCE λ_1 is given by

$$\lambda_1 = \omega_k \text{Re}[\lambda]_{\max} = \frac{3}{8} \omega_k \beta\epsilon. \quad (73)$$

If we calculate λ_1 for the case of $N=64$, $k=43$, and $\epsilon = 0.01$ according to Eq. (73), we obtain $\lambda_1 = 6.5 \times 10^{-3}$. This is in good agreement with the numerical value $\lambda_1 = 5.9 \times 10^{-3}$ in Fig. 3(a). The agreement becomes better as ϵ decreases. This comparison validates our analytical computation of the LCE. From Eq. (29), we can obtain the ϵ scaling of the induction time T as

$$T \sim \frac{1}{\omega_k \beta\epsilon} \sim \epsilon^{-1}. \quad (74)$$

The induction time T is proportional to the inverse of ϵ . Moreover, T depends on the frequency ω_k of the initially excited mode and thus becomes smaller for higher-frequency mode excitation. The range μ_0 for positive $\text{Re}[\lambda]$ can also be easily found as

$$\mu_0 = \sqrt{\frac{3\beta\epsilon}{2}}. \quad (75)$$

We can see that μ_0 decreases with decreasing ϵ . This means that the number of modes with positive exponential growth rates decreases as ϵ decreases. If ϵ is small enough and the growth rate of the $m=1$ pair of modes becomes zero, namely, $\mu_0 < \pi/2N$, then all of the modes become stable and the induction time T diverges. This threshold energy density ϵ_c determined from $\mu_0 < \pi/2N$ is obtained for large N as

$$\epsilon_c = \frac{\pi^2}{6\beta N^2}. \quad (76)$$

This shows that ϵ_c decreases as the system size N increases, $\epsilon_c \sim N^{-2}$, and vanishes in the thermodynamic limit $N \rightarrow \infty$. Equation (76) also shows that the threshold does not depend on the initially excited mode number k , except in the cases of $k=1, N/2$, and $N-1$.

A similar expression $\epsilon_c = \pi^2/3\beta N^2$ has been obtained for the stability threshold of the zone-boundary mode although periodic boundary conditions were employed in Refs. [23,25,26]. Moreover, for a generic large k mode excitation and in the case of periodic boundary conditions, Berman and Kolovskii obtained an expression for the exponential growth rate of the perturbation similar to our lowest order result Eq. (69), different only with respect to the factors, and the stability threshold $\epsilon_c = \pi^2/3\beta N^2$ by means of a different approximation [27]: they retained only the resonant terms and made the narrow-packet approximation in Hamiltonian (5) to obtain an integrable Hamiltonian, and examined the linear stability of a plane wave solution of the integrable Hamiltonian system. Our result shows that their approximation is reasonable up to the lowest order.

The higher-order terms in Eq. (60) are important for large ϵ . Equation (69) shows that $\text{Re}[\lambda]$ does not depend on the initially excited mode k in the lowest-order expansion. However, k dependence of $\text{Re}[\lambda]$ appears as ϵ increases. The eigenvalue λ is a function of m/N , k/N , and ϵ . In Figs. 6(a)–6(c), $\text{Re}[\lambda]$ obtained from Eq. (60) is plotted as a function of m/N and ϵ for $k/N = 0.289, 0.664$, and 0.867 , respectively. The shape of $\text{Re}[\lambda]$ is apparently different among these results in the large ϵ regime. The number of unstable modes strongly depends on k . It is interesting that in the case

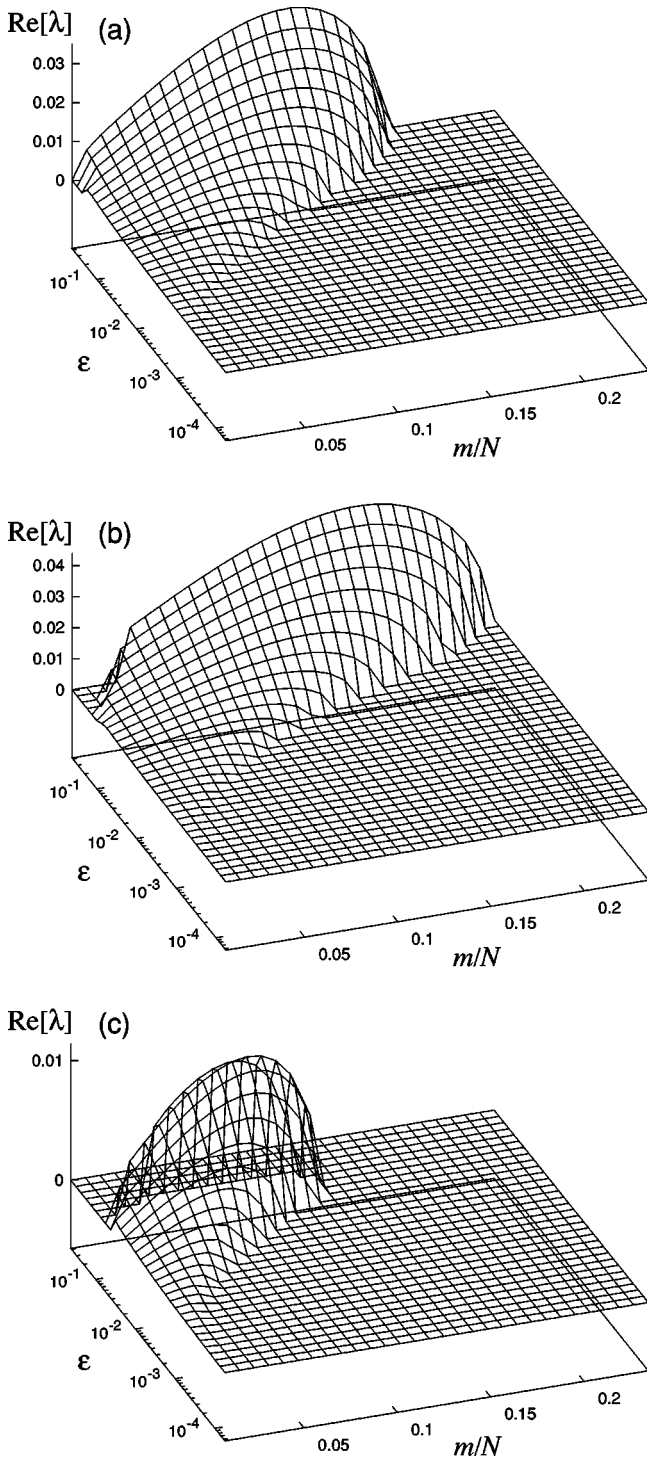


FIG. 6. $\text{Re}[\lambda]$ as a function of m/N and ϵ . (a) $k/N=0.289$. (b) $k/N=0.664$. (c) $k/N=0.867$.

of $k/N=0.867$ all the modes become stable when ϵ exceeds some critical value: the parametric resonance between $k \pm m$ modes is suppressed. In this ϵ regime, the induction time T becomes somewhat longer in numerical experiments and the energy exchange may be driven by another parametric resonance mechanism.

V. NUMERICAL EXPERIMENTS

We performed numerical experiments in order to verify the above theoretical results. A numerical integration of the

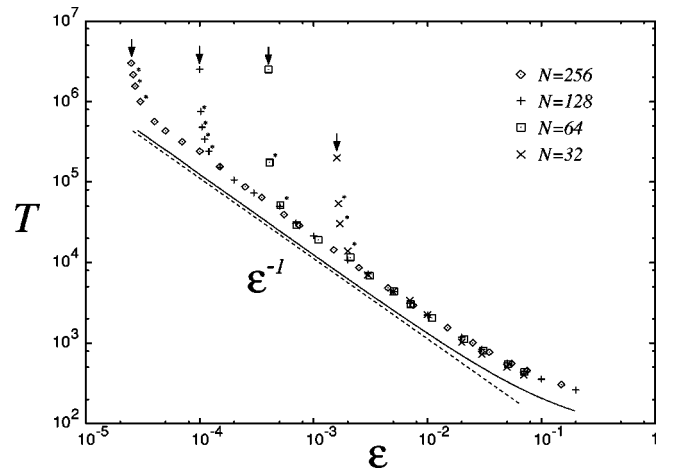


FIG. 7. Induction time T plotted versus energy density ϵ . System size is $N=32, 64, 128$, and 256 , and modes of $k=21, 43, 85$, and 171 ($k \approx 2N/3$) are initially excited. A reference line of power law ϵ^{-1} (dashed line) and a reference line obtained from $\text{Re}[\lambda]_{\max}$ of the full order expression of λ Eq. (60) (solid line) are also drawn.

equations of motion (2) was performed by using the leapfrog algorithm because of its symplectic nature and simplicity. The nonlinear coupling strength β was set as $\beta=1$ in all the following numerical experiments. We use an initial condition consisting of an almost single-mode excitation: at the initial time, most of the energy is given to a single mode of wave number k and only a small amount of energy [$(1 \times 10^{-10})\epsilon$] is placed in every other mode. The energy is contained in kinetic form initially. This initial condition is physically more natural and generic than the exact single-mode excitation.

We define the induction time T as the time when the energy $E_k(t)$ of the initially excited mode decreases to 50% of the initial value, i.e., $E_k(T)=0.5E_k(0)$ [this is equivalent to $\Delta E(T) \approx 0.5E_k(0)$]. For very small ϵ , the maximum amount of energy transferred from the initially excited mode to the others never exceeds 50% of $E_k(0)$. In such a case, we define T as the time when $E_k(t)$ shows a perceptible decrease and takes a minimum value for the first time [cf. Fig. 11(b) below]. This case is marked by * in the following figures. Moreover, for further small ϵ 's, $E_k(t)$ does not show a perceptible decrease until the end of the calculation [cf. Fig. 11(a) below]. This case is marked by an arrow in the following figures. The induction time T is calculated for N in the range 32 to 256. The initially excited mode number is set to $k \approx 2N/3$: $k=21, 43, 85$, and 171 for $N=32, 64, 128$, and 256 , respectively. Figure 7 shows the induction time T plotted as a function of ϵ for several N 's, a reference line of the power law ϵ^{-1} , and a reference line obtained from $\text{Re}[\lambda]_{\max}$ of the full order expression of λ Eq. (60) ($T \sim 1/\text{Re}[\lambda]_{\max}$). Here the numerical results for T are clearly in good agreement with the power law $T \sim \epsilon^{-1}$ although the numerical results become different from the power law as ϵ becomes sufficiently large, roughly $\epsilon > 0.01$. In the range $\epsilon > 0.01$, T decreases more slowly than ϵ^{-1} with an increase in ϵ . The full order scaling law is in good agreement with this numerical result.

The induction time T is not (or at least only weakly) dependent on N . The spacing between two neighboring modes

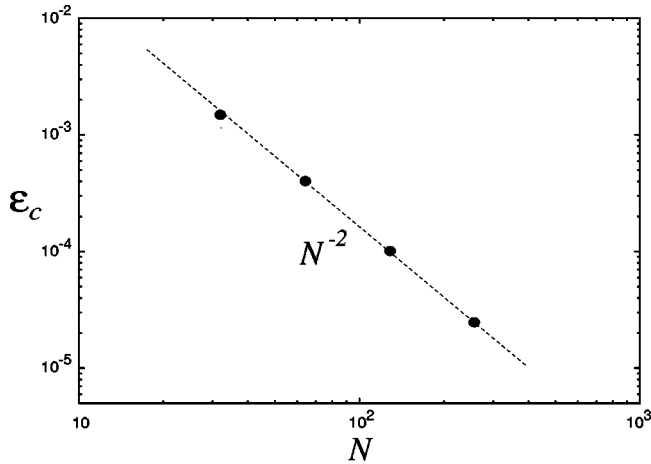


FIG. 8. Threshold energy density ϵ_c plotted against N . The line for the theoretical estimation $\epsilon_c = \pi^2/6\beta N^2$ is also shown.

becomes more dense in k/N space with an increase in N . Consequently, k_{max}/N approaches the limiting value $k/N \pm \sqrt{3\beta\epsilon}/\pi$ with increasing N in Eq. (72), and thus λ_1 also approaches the corresponding limiting value given by Eq. (73), which depends only on k/N and ϵ . Therefore, T converges to a certain value with an increase in N under fixed k/N and ϵ . This coincides with the above numerical observation.

In Fig. 7, the induction time T displays an apparently divergent behavior as ϵ decreases. We define the threshold energy density ϵ_c using the value of ϵ at the points marked by arrows. The threshold energy density ϵ_c decreases with increasing N . Figure 8 shows a plot of threshold ϵ_c against N and a theoretical line $\epsilon_c = \pi^2/6\beta N^2$, Eq. (76). They completely agree with each other.

The energy growth rates are different between the modes as shown in Fig. 1. In Fig. 9, the difference $k_{max} - k$ between the mode number of the mode exhibiting the largest energy growth rate in the numerical experiments and that of the

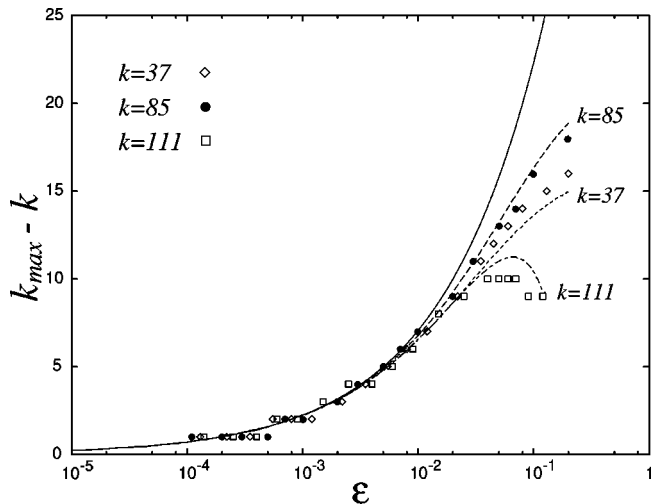


FIG. 9. Mode with largest energy growth rate. $k_{max} - k$ is plotted against ϵ . Parameters are $N=128$ and $k=37, 85,$ and 111 . The theoretical line $k_{max} - k = N\sqrt{3\beta\epsilon}/\pi$ (solid line) and three theoretical lines obtained from $\text{Re}[\lambda]$ of the full order expression of λ , Eq. (60), are also shown.

initially excited one is plotted against ϵ . We note that the energy growth rate of each mode was measured in an early part of the induction period [cf. Figs. 1 and 11(b)–11(d) below]. We show the results for $k=37, 85,$ and 111 in the case of $N=128$, which correspond to the cases in Figs. 6(a)–6(c), respectively. In Fig. 9, the lowest-order theoretical result $k_{max} - k = N\sqrt{3\beta\epsilon}/\pi$ obtained from Eq. (72) is plotted with a solid line and three theoretical lines obtained from the mode number k_{max} that maximizes $\text{Re}[\lambda]$ of the full order expression of λ Eq. (60) are also plotted. The results are symmetric with respect to the line $k_{max} - k = 0$ although we show only the results for $k_{max} - k > 0$. Good agreement between the numerical and lowest order theoretical result is observed for small ϵ , but the agreement becomes rather worse with an increase in ϵ . Moreover, in the large ϵ regime, the numerical results show that the difference $k_{max} - k$ strongly depends on k . The full order theoretical estimations coincide with the numerical results even in this large ϵ regime.

Figures 10(a)–10(c) present numerical results of T plotted against ϵ for various initially excited mode numbers k , where $N=128$, and (a), (b), and (c) refer to $k=3, 51,$ and 125 , respectively. The reference lines of the power law ϵ^{-1} are also shown and this power law is validated in these cases. Note that a discrepancy from the power law appears at smaller ϵ in the case of $k=3$ and 125 than in the case of $k=51$ and 85 . These modes, which are too close to 1 or N , do not have a sufficient number of pairs of modes $k \pm m$: only $m=1, 2$ are allowed in these cases. Therefore, the present analysis does not apply when $k_{max} - k \geq 3$. This is the main reason why the discrepancy from the power law appears for smaller ϵ . In addition, some other mechanism suppressing the parametric instability, which is not included in the approximate result Eq. (69), seems to exist. Comparing Figs. 7, 10(a), 10(b), and 10(c), we can also confirm that T becomes smaller for higher-frequency mode excitation. The thresholds in ϵ in all three cases coincide with the theoretical value $\epsilon_c = 1.004 \times 10^{-4}$, which is calculated from Eq. (76) for $N=128$. This agrees with the theoretical prediction that the threshold does not depend on the initially excited mode number k .

Let us briefly mention here the reason why we used the second order averaging method instead of the first order one. If we calculate the LCE using the first order averaging method, we obtain zero LCE for any initial excitation of $k \leq N/2$. However, this result is apparently inconsistent with the preceding numerical results for $k=3$ and 51 . The first order averaging method is considered inadequate for appropriately calculating the LCE. Therefore, we used the second order one.

We proceed to discuss the energy exchange process following the induction period in some energy density regimes. Figures 11(a)–11(d) show the time evolution of mode energies in different energy density regimes: we plot only some of the mode energies E_i for graphical reasons. Figures 11(a), 11(b), 11(c), and 11(d) refer to $\epsilon = 1 \times 10^{-4}, 2 \times 10^{-4}, 7 \times 10^{-4},$ and 1×10^{-2} , respectively. The other parameters are $N=128$ and $k=85$.

In Fig. 11(a), mode energies except for $i=85$ do not grow but remain small over the long period. The other mode en-

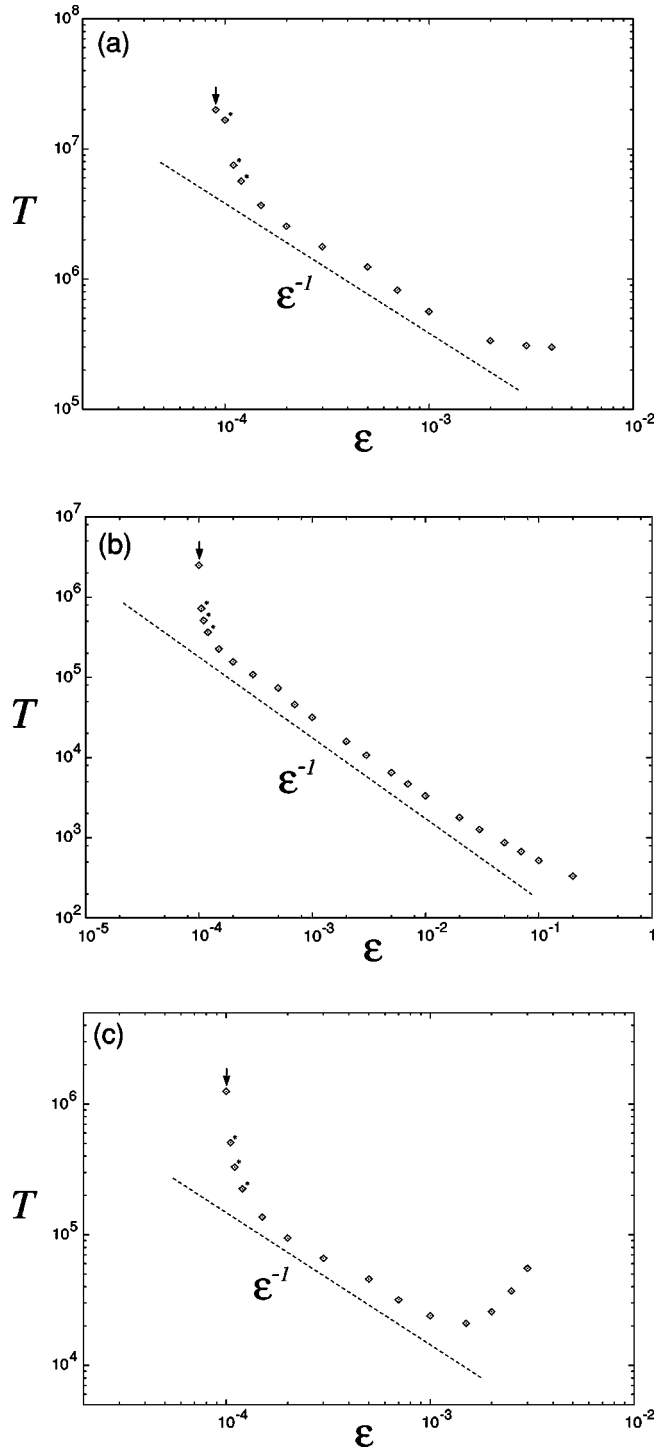


FIG. 10. Induction time T plotted versus energy density ϵ . System size is $N = 128$. (a) $k = 3$. (b) $k = 51$. (c) $k = 125$. A reference line of power law ϵ^{-1} is also drawn.

ergies not shown in the figure also remain small. The energy density of this figure, $\epsilon = 1 \times 10^{-4}$, is slightly smaller than the theoretical threshold, $\epsilon_c = 1.004 \times 10^{-4}$. Equation (30) indicates that the phase point separation $\Gamma(nt_0) - \Gamma(0)$ is bounded by a small value; thus, every E_i of the modes other than the initially excited one remains of the order of its small value at the initial stage over the infinite time when $\epsilon < \epsilon_c$. This suggests that Kolmogorov-Arnold-Moser (KAM) tori exist near the pseudoperiodic orbit in phase space when ϵ

$< \epsilon_c$. The numerical result in Fig. 11(a) coincides with the theoretical result and indicates that the KAM tori exist. In the range $\epsilon < \epsilon_c$, the system retains the initially excited mode structure over infinite time, and it therefore never relaxes to an energy equipartition state. In this connection, it has been shown recently that, if the FPU β system starts from a high-frequency mode excitation, the system relaxes to an energy equipartition state via a spatially localized oscillating structure called a *chaotic breather*, which is spontaneously created in the system after the breakup of the initially excited high-frequency mode structure [28–30]. The present result indicates that there is an energy threshold for creating the chaotic breather since the chaotic breather is never created, at least, below ϵ_c . It may be interesting to study the threshold for creating the chaotic breather, in other words, when the path from a single high-frequency mode state to the chaotic breather state is created in phase space.

Figure 11(b) shows a graph for $\epsilon = 2 \times 10^{-4}$, which slightly exceeds ϵ_c . In this figure, only mode 86 grows exponentially and the others remain small in the early stage of the induction period. This coincides with the two-mode AVE analysis. However, the other modes begin to grow exponentially after a time, and begin to differ from the theoretical result. E_{84} and E_{86} have increased to a certain degree when the growth of these modes begins. It may be conceivable that small-amplitude oscillations of modes 84 and 86, which are neglected in the pseudoperiodic orbit approximation, lead to another parametric resonance mechanism resulting in the exponential growth of modes other than modes 84 and 86. After the induction period, E_{86} alternately repeats rather regular exponential decreases and increases. The other modes also exhibit repeated exponential decreases and increases, following mode 86. It should be noted that E_{87} , E_{88} , and E_{89} fluctuate chaotically when they become small after the exponential decrease. This alternate decrease and increase in E_i accompanied by chaotic fluctuation suggests that a very thin stochastic separatrix layer is formed. Since a nonconjugate pair of the eigenvalues merges as shown in Fig. 4, a Krein collision may occur on a periodic orbit near the pseudoperiodic orbit. The largest Lyapunov exponent calculated for the motion in the thin stochastic separatrix layer is $\lambda_{Lyap} = 4 \times 10^{-6}$. From the above numerical observation, ϵ_c is regarded as a threshold for the appearance of weakly chaotic motion in the thin stochastic separatrix layer. In this connection, a threshold for the formation of a stochastic separatrix layer under low-frequency mode excitation was obtained by numerically investigating a reduced four-mode Hamiltonian system in [16]. Their result agrees with our analytical result for ϵ_c . We can see from the figure that the characteristic frequency of the exponential decrease and increase in E_i is roughly estimated as $\Omega_b \approx 1/2T$. From Eqs. (29) and (73), Ω_b can be estimated as $\Omega_b \approx \omega_k \beta \epsilon$. For an initial excitation of the small k mode, this can be approximated by $\Omega_b \approx k \beta \epsilon / N$. This also agrees with the characteristic frequency of beat oscillation due to the resonant interaction of a few low-frequency modes, which is obtained by using the reduced four-mode Hamiltonian in [16]. A numerical calculation over a longer time scale shows that energy is shared by only a small number of modes and is not transferred to the other modes on a computationally observable time scale. In this sense, the chaos in this small ϵ range is local chaos. More-

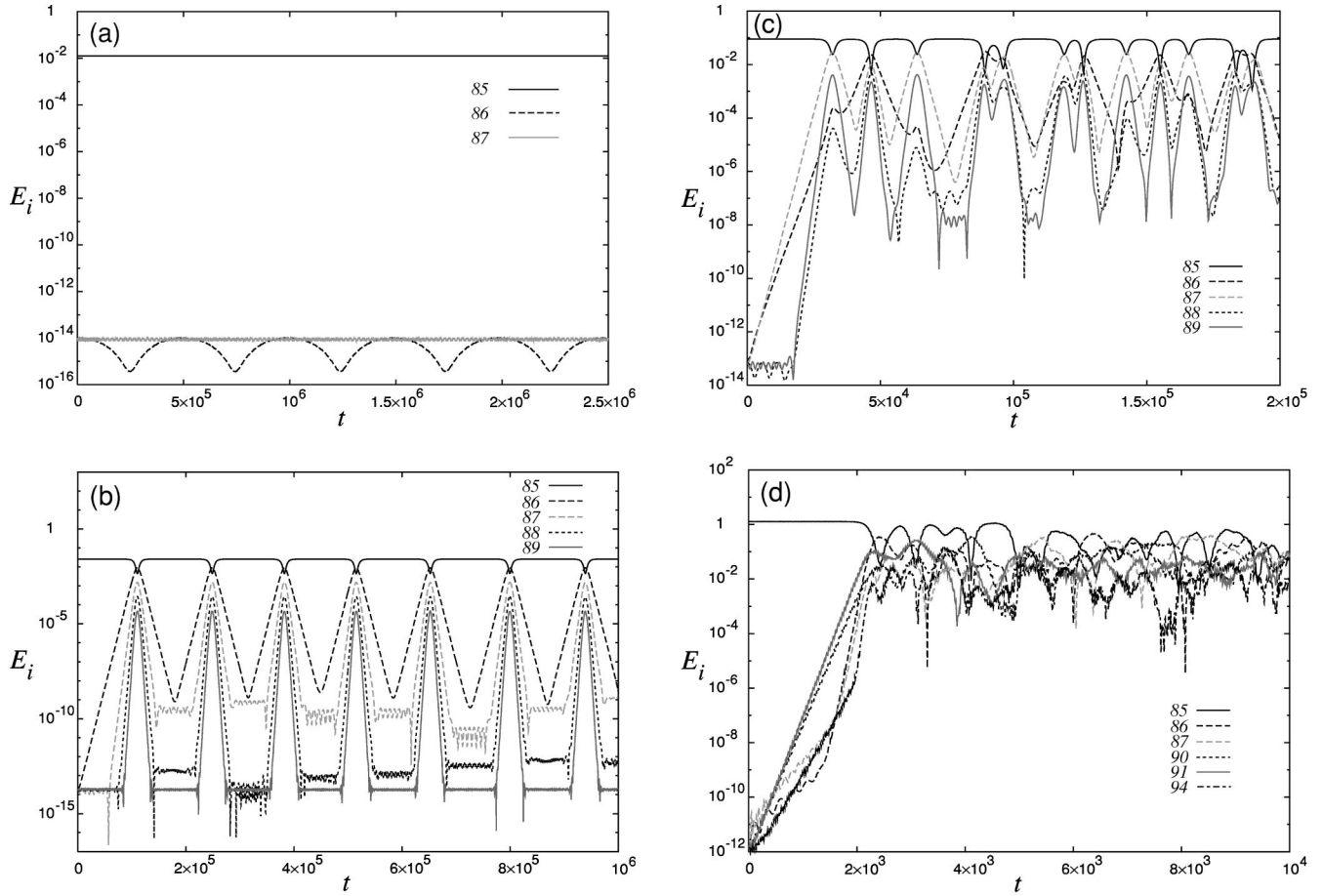


FIG. 11. Mode energies E_i plotted versus time t . $N=128$ and $k=85$. (a) $\epsilon=1 \times 10^{-4}$. (b) $\epsilon=2 \times 10^{-4}$. (c) $\epsilon=7 \times 10^{-4}$. (d) $\epsilon=1 \times 10^{-2}$.

over, as characterized by the small Lyapunov exponent, it is very weak chaos.

As ϵ increases, the number of modes sharing energy becomes larger and the motion also become more chaotic. However, energy equipartition does not seem to be achieved on a computationally observable time scale for relatively small ϵ . The equipartition time scale might be infinite. Figure 11(c) shows a graph for $\epsilon=7 \times 10^{-4}$, which is an example for such a value of ϵ . Apparently chaotic energy exchange occurs after the induction period and the chaotic motion is stronger than that of Fig. 11(b). However, as seen in a longer calculation, energy is shared by a subset of modes and equipartition is not achieved even in a long numerical calculation. The motion is still restricted to the subset of modes. In this sense, the chaos of this ϵ range is strong local chaos.

As ϵ increases further, the equipartition comes to occur on short time scales. In this sense, the chaotic motion becomes global. The mode energy exchange for the relatively large energy density of $\epsilon=1 \times 10^{-2}$ is shown in Fig. 11(d). Strongly chaotic energy exchange occurs after the induction period. In this case, energy is distributed to every mode on a rather short, or computationally observable, time scale. The equipartition time decreases with an increase in ϵ . Recently, it has been shown that in a relatively large ϵ regime the equipartition time scales as ϵ^{-3} [31].

VI. CONCLUSIONS

We have carried out an analytical study of the induction phenomenon in the FPU β model relating the energy exchange process to linear instability of the orbit, and have shown that parametric resonance in the AVE can describe the induction phenomenon quite well. Our theoretical study is based on an analytical computation of the LCE of the AVE using a second order averaging method. In order to perform the analytical computation, we used the two-mode approximation to the AVE. The two-mode approximation analysis applies to the initial excitation of any mode except for the three modes $k=1$, $N/2$, and $N-1$.

The results are summarized as follows: (1) the energy density scaling of the induction time is given by $T \sim \epsilon^{-1}$ and T becomes smaller for higher-frequency mode excitation; (2) there is a threshold energy density ϵ_c such that the induction time diverges when $\epsilon < \epsilon_c$ and it is given by $\epsilon_c = \pi^2/6\beta N^2$ for large N ; (3) the threshold ϵ_c vanishes as $\epsilon_c \sim N^{-2}$ in the limit $N \rightarrow \infty$; (4) the threshold ϵ_c does not depend on the mode number k that is excited in the initial condition; (5) the two modes $k \pm m$ have the largest exponential growth rate and m increases with increasing ϵ as $m/N = \sqrt{3\beta\epsilon}/\pi$. These analytical results are thoroughly verified in numerical experiments. The above estimations $T \sim \epsilon^{-1}$ and $m/N = \sqrt{3\beta\epsilon}/\pi$ are correct only in the small ϵ regime since they are obtained from the lowest-order expansion of λ . Therefore, the agree-

ment between these estimations and the numerical results becomes worse as ϵ increases. The estimations for T and m/N based on the full order expression of λ are in good agreement with the numerical results even in the large ϵ regime.

We have also discussed the energy exchange process after the induction period in some energy density regimes, based

on the numerical results. We show that KAM tori exist near the pseudoperiodic orbit when $\epsilon < \epsilon_c$, and ϵ_c is regarded as the threshold for formation of a thin stochastic separatrix layer near the pseudoperiodic orbit. Apparently, chaotic energy exchange begins to occur just after the induction period when ϵ becomes large.

-
- [1] E. Fermi, J. Pasta, and S. Ulam, in *Collected Papers of E. Fermi*, edited by E. Segré (University of Chicago Press, Chicago, 1965).
- [2] L. Casetti, M. Cerruti-Sola, M. Pettini, and E. G. D. Cohen, *Phys. Rev. E* **55**, 6566 (1997).
- [3] D. L. Shepelyansky, *Nonlinearity* **10**, 1331 (1997).
- [4] F. M. Izrailev and B. V. Chirikov, *Dokl. Akad. Nauk SSSR* **166**, 57 (1966) [*Sov. Phys. Dokl.* **11**, 30 (1966)].
- [5] A. J. Lichtenberg and M. A. Lieberman, *Regular and Chaotic Dynamics* (Springer, Berlin, 1992).
- [6] G. M. Zaslavsky, *Chaos in Dynamic System* (Harwood Academic, Amsterdam, 1987).
- [7] K. Yoshimura, *Phys. Rev. E* **54**, 5766 (1996).
- [8] K. Yoshimura, *Phys. Rev. E* **59**, 3641 (1999).
- [9] M. Pettini and M. Landolfi, *Phys. Rev. A* **41**, 768 (1990).
- [10] M. Pettini and M. Cerruti-Sola, *Phys. Rev. A* **44**, 975 (1991).
- [11] K. Yoshimura, *Physica D* **104**, 148 (1997).
- [12] M. Pettini, *Phys. Rev. E* **47**, 828 (1993).
- [13] L. Casetti and M. Pettini, *Phys. Rev. E* **48**, 4320 (1993).
- [14] L. Casetti, R. Livi, and M. Pettini, *Phys. Rev. Lett.* **74**, 375 (1995).
- [15] L. Casetti, C. Clementi, and M. Pettini, *Phys. Rev. E* **54**, 5969 (1996).
- [16] J. De Luca, A. J. Lichtenberg, and S. Ruffo, *Phys. Rev. E* **51**, 2877 (1995).
- [17] N. Ooyama, N. Hirotsu, and N. Saito, *J. Phys. Soc. Jpn.* **27**, 815 (1969).
- [18] N. Saito, N. Ooyama, Y. Aizawa, and H. Hirooka, *Suppl. Prog. Theor. Phys.* **45**, 209 (1970).
- [19] N. Saito, N. Hirotsu, and A. Ichimura, *J. Phys. Soc. Jpn.* **39**, 1431 (1975).
- [20] G. Christie and B. I. Henry, *Phys. Rev. E* **58**, 3045 (1998).
- [21] N. N. Bogoliubov and Y. A. Mitropolsky, *Asymptotic Methods in the Theory of Nonlinear Oscillations* (Gordon and Breach, New York, 1961).
- [22] N. Budinsky and T. Bountis, *Physica D* **8**, 445 (1983).
- [23] P. Poggi and S. Ruffo, *Physica D* **103**, 251 (1997).
- [24] R. L. Bivins, N. Metropolis, and J. R. Pasta, *J. Comput. Phys.* **12**, 65 (1973).
- [25] T. Dauxois, S. Ruffo, and A. Torcini, *Phys. Rev. E* **56**, R6229 (1997).
- [26] T. Dauxois, S. Ruffo, and A. Torcini, *J. Phys. IV* **8**, 147 (1998).
- [27] G. P. Berman and A. R. Kolovskii, *Zh. Éksp. Teor. Fiz.* **87**, 1938 (1984) [*Sov. Phys. JETP* **60**, 1116 (1984)].
- [28] T. Cretegny, T. Dauxois, S. Ruffo, and A. Torcini, *Physica D* **121**, 109 (1998).
- [29] K. Ullmann, A. J. Lichtenberg, and G. Corso, *Phys. Rev. E* **61**, 2471 (2000).
- [30] Y. A. Kosevich and S. Lepri, *Phys. Rev. B* **61**, 299 (2000).
- [31] J. De Luca, A. J. Lichtenberg, and S. Ruffo, *Phys. Rev. E* **60**, 3781 (1999).